LA-UR- 08-7561

Approved for public release; distribution is unlimited.

Title:	Suppressing Nonphysical Overheating with a Modified Implicit Monte Carlo Method for Time-Dependent Radiative Transfer (U)
Author(s):	Ryan G. McClarren, CCS-2 Todd J. Urbatsch, CCS-2
Intended for:	Journal of Computational Physics

Form 836 (7/06)

Los Alamos
NATIONAL LABORATORY
research note
Computer and Computational Sciences Division
CCS-2:Computational Physics Group

To/MS: Distribution
From/MS: Ryan G. McClarren/CCS-2 D413
Todd J. Urbatsch/CCS-2 D409
Phone/FAX: (505)665–1397
Symbol: CCS-2:08-57 (U)
Date: November 20, 2008

Subject: Suppressing Nonphysical Overheating with a Modified Implicit Monte Carlo Method for Time-Dependent Radiative Transfer

Executive Summary

In this note we develop a robust implicit Monte Carlo (IMC) algorithm based on more accurately updating the linearized equilibrium radiation energy density. The method does not introduce oscillations in the solution and has the same limit as $\Delta t \to \infty$ as the standard Fleck and Cummings IMC method. Moreover, the approach we introduce can be trivially added to current implementations of IMC by changing the definition of the Fleck factor. Using this new method we develop an adaptive scheme that uses either standard IMC or the modified method basing the adaptation on a zero-dimensional problem solved in each cell. Numerical results demonstrate that the new method alleviates both the nonphysical overheating that occurs in standard IMC when the time step is large and significantly diminishes the statistical noise in the solution.

1 Introduction

Originally introduced by Fleck and Cummings [1], the implicit Monte Carlo (IMC) method is a stochastic means of solving the thermal radiative transfer equations. It manipulates the nonlinear equations describing thermal radiative transfer to get a linearized transport equation that can be solved using the standard Monte Carlo techniques for linear transport. Whereas for linear transport the Monte Carlo solution is exact modulo the statistical noise, IMC has truncation error in the solution. These errors arise from the linearization of the material energy equation and from approximately time integrating the material energy equation. Also, spatial error is introduced by the necessity of having a spatial grid to describe the material temperature.

A particularly vexing problem with IMC is the potential for the solution to nonphysically violate the maximum principle that solutions to time-dependent radiative transfer physically obey [2]. This maximum principle states that if the material and radiation temperatures have initial and boundary data that lie within a temperature bounds, then the solution forever will lie between these bounds [3, 4]. Both Larsen and Mercier [2] and Mosher and Densmore [5] have attempted to develop time step controls. The time step limits derived were prohibitively small and are often more restrictive than necessary.

The violation of the maximum principle by IMC has been shown in infinite medium problems by Densmore and Larsen [6] where the material temperature becomes hotter than the maximum initial radiation temperature in one time step. On Marshak wave problems with a large time step, the IMC solution can have the material temperature higher than the boundary temperature. A more subtle overheating phenomenon in IMC solutions occurs when given initial data with the radiation temperature above the material temperature, the IMC solution nonphysically "flips" these temperatures [7].

In a coupled radiation-hydrodynamics simulations such overheating can cause severe problems. In such a calculation if the material temperature nonphysically overheats, as in the Fleck and Cummings solutions, the hydrodynamic solution will incorrectly evolve because of the too large amount of energy deposited in the material by the radiation. For example, the incorrect evolution of the hydrodynamics can manifest itself as spurious ablation or shock formation.

Various methods have attempted to correct certain errors in the IMC method. The Carter-Forest method [8] exactly solves the linearized material energy equation through a Monte Carlo procedure, and the symbolic implicit Monte Carlo (SIMC) method [9, 10] does not have linearization error but does introduce a time discretization error.

Despite the potential benefits of other methods, IMC is the stochastic method used most often for simulating thermal radiative transfer. Below we derive a method that is similar to the Fleck and Cummings IMC method in that it represents the absorption/emission process through effective absorption and scattering, but more accurately integrates the linearized material energy equation. This higher order method can be easily implemented in current IMC simulations simply by changing the definition of the Fleck factor. With the modified IMC method we devise an adaptive scheme to determine how much effective absorption or scattering there will be in the problem. This adaptive method takes the beginning of time step radiation and material temperatures in each cell and solves a zero-dimensional transport problem via standard IMC. If the material temperature in this 0-D solution is greater than the equilibrium temperature, the modified method is used to suppress this overheating.

2 Derivation for the Grey Case

It is useful to introduce the Fleck and Cummings [1] (IMC) method before we derive our modified method. After discussing this standard method, we will develop our new approach.

2.1 Standard IMC Method

We begin with the equations for grey thermal radiative transfer without scattering [1],

$$\frac{1}{c}\frac{\partial I}{\partial t} + \hat{\Omega}\cdot\nabla I + \sigma I = \frac{1}{4\pi}\sigma a c T^4 \,, \tag{1a}$$

$$\frac{\partial u_{\mathrm{m}}}{\partial t} = \sigma\left(\int_{4\pi} I\, d\hat{\Omega} - acT^4\right) + S \,. \tag{1b}$$

In these equations the specific intensity of radiation is denoted by $I(\mathbf{x}, \hat{\Omega}, t)$, T is the material temperature, u_{m} is the material energy density, $\hat{\Omega}$ is the direction of flight, a is the radiation constant, c is the speed of light, S is an arbitrary source function, and $\sigma(x, T)$ is the opacity of the material and has units of inverse length. Equation (1a) models the transport of the radiation through the material medium, and Eq. (1b) governs the change in material temperature as a result of radiation being absorbed and emitted by the material as well as the source S.

To derive an implicit Monte Carlo method for these equations we will define the equilibrium energy density variable as

$$u_{\mathrm{r}} = aT^4 \,, \tag{2}$$

In words u_{r} is the value of the radiation energy density when the material and radiation are in equilibrium. As is standard, we also write

$$\frac{\partial u_{\mathrm{m}}}{\partial u_{\mathrm{r}}} = \beta^{-1} \,. \tag{3}$$

In the simple case of constant heat capacity, the material energy density is given by $u_{\mathrm{m}} = \rho c_v T$ and $\beta = \frac{4aT^3}{\rho c_v}$. Using our newly defined variables we can rewrite Eq. (1) as

$$\frac{1}{c}\frac{\partial I}{\partial t} + \hat{\Omega}\cdot\nabla I + \sigma I = \frac{1}{4\pi} c\sigma u_{\mathrm{r}} \,, \tag{4a}$$

$$\frac{\partial u_{\mathrm{r}}}{\partial t} = \beta\sigma\left(\int_{4\pi} I\, d\hat{\Omega} - cu_{\mathrm{r}}\right) + \beta S \,. \tag{4b}$$

The goal of an implicit Monte Carlo method is to get an implicit definition of u_r from Eq. (4b) to linearize Eq. (4a) allowing a Monte Carlo solution of the radiation transport.

The Fleck and Cummings procedure averages Eq. (4b) over a time step as

$$\frac{u_r^{n+1} - u_r^n}{\Delta t} = \frac{1}{\Delta t}\int_{t_n}^{t_{n+1}} dt \left[\beta\sigma\left(\int_{4\pi} I\, d\hat{\Omega} - cu_r\right) + \beta S\right] , \tag{5}$$

where the superscripts denote the time level. Then the average value of u_r is written as an interpolation between the beginning and end of step values

$$\tilde{u}_r \equiv \frac{1}{\Delta t}\int_{t_n}^{t_{n+1}} dt\, u_r \approx \alpha u_r^{n+1} + (1-\alpha)u_r^n . \tag{6}$$

Using the definition of the $\tilde{u}_r$ in Eq. (5) gives

$$u_r^{n+1} = u_r^n + \int_{t_n}^{t_{n+1}} dt\, \beta\sigma \int_{4\pi} I\, d\hat{\Omega} - c\Delta t\bar{\beta}\bar{\sigma}(\alpha u_r^{n+1} + (1-\alpha)u_r^n) + \bar{\beta}\Delta t\bar{S} , \tag{7}$$

where $\bar{(\cdot)}$ denotes a properly time-averaged quantity, $\alpha \in [0,1]$ is the implicitness factor, and the superscripts denote the time level. In practice α is almost always set to unity because smaller values of α can lead to oscillatory behavior in the solution although $\alpha = 1/2$ gives a second-order update. Also, $\bar{\beta}$ and $\bar{\sigma}$ are generally evaluated at the n time level. A consistent approximation to Eq. (7) is

$$u_r^{n+1} = u_r^n + \Delta t\bar{\beta}\bar{\sigma}\int_{4\pi} I\, d\hat{\Omega} - c\Delta t\bar{\beta}\bar{\sigma}(\alpha u_r^{n+1} + (1-\alpha)u_r^n) + \bar{\beta}\Delta t\bar{S} , \tag{8}$$

where the error in this approximation is $O(\Delta t)$.

Equation (7) can be rewritten as

$$u_r^{n+1} = fu_r^n + \frac{(1-f)}{c}\left(\int_{4\pi} I\, d\hat{\Omega} + \frac{1}{\sigma}S\right) , \tag{9}$$

with

$$f = \frac{1}{1+\alpha\beta\sigma c\Delta t} , \tag{10}$$

and for convenenience we have dropped the overbars from β, S, and σ. The expression for u_r^{n+1} from Eq. (9) is then substituted into the transport equation, Eq. (4a), to get the linear transport equation to be solved by Monte Carlo:

$$\frac{1}{c}\frac{\partial I}{\partial t} + \hat{\Omega}\cdot\nabla I + \sigma I = \frac{1}{4\pi}(1-f)\sigma\int_{4\pi} I\, d\hat{\Omega} + \frac{1}{4\pi}\left(c\sigma f u_r + (1-f)S\right) . \tag{11}$$

This tranport equation has some interesting properties. As a result of the procedure for updating u_r^{n+1}, Eq. (11) has effective scattering and absorption coefficients given by

$$\sigma_s = (1-f)\sigma , \qquad \sigma_a = f\sigma . \tag{12}$$

Equation (11) can be solved with a standard linear Monte Carlo solution technique. We also note that the factor f is bounded by $0 \le f \le 1$ and that as $\Delta t \to \infty$ the value of f goes to zero, such that there is no effective absorption and the material energy will not change over a time step.

2.1.1 Approximations in IMC

We now briefly summarize the approximations in the Fleck and Cummings procedure. First, we note that the material energy equation was linearized by approximating the value of β and σ with a single value; in reality these values change nonlinearly with the material energy. This approximation is hard to avoid because we generally desire a linear transport equation to solve via Monte Carlo. It would be possible to define an iterative procedure to remove the linearization error by linearizing Eq. (1b) and solving a linear transport equation and updating β and σ each iteration. Such an iterative method, called a Picard iteration, is used in deterministic methods, might be prohibitively expensive because it would involve several Monte Carlo solutions per time step. The linearization error is also addressed by the symbolic implicit Monte Carlo method (SIMC) [9,10] where Eq. (1b) is not linearized but σ .

The other main approximation in the Fleck and Cummings IMC method is that the instantaneous intensity, I, is used in the definition of u_{r}^{n+1} in going from Eq. (7) to Eq. (8), which is equivalent to assuming that the time dependence of I does not influence the emission process. Under this assumption the re-emission process is instantaneous, which gives the effective scattering term, and the strength of the emission source does not change over the time step. The Carter-Forest method [8] addresses this issue by defining time dependent source and re-emission terms that are sampled in the Monte Carlo solution of the tranport equation.

2.2 High-Order Update for u_{r}^{n+1}

Despite its shortcomings, the Fleck and Cummings IMC method is widely used to solve time-dependent radiative transfer problems. In this study we do not address the approximations in IMC discussed above (linearization and instantaneous absorption/emission). Rather, we will address the temporal truncation error in the IMC method.

The value of u_{r}^{n+1} given by Eq. (9) is a first-order in Δt approximation to the solution of Eq. (4b). The method we introduce in this study hinges on the fact that it is possible to exactly integrate Eq. (4b) under the assumptions of the IMC approach.

To update u_{r}^{n+1} we do not make an approximation to the average value of u_{r} over a time step but instead write Eq. (7) as

$$u_{\mathrm{r}}^{n+1} - u_{\mathrm{r}}^{n} = \beta\sigma \int_{t_n}^{t^{n+1}} \left(\int_{4\pi} I \, d\hat{\Omega} - c u_{\mathrm{r}} \right) dt + \Delta t \beta S \, . \tag{13}$$

The exact solution of Eq. (13) is given by

$$u_{\mathrm{r}}^{n+1} = e^{-\beta\sigma c\Delta t} u_{\mathrm{r}}^{n} - e^{-\beta\sigma c\Delta t} \beta\sigma \int_{t_n}^{t^{n+1}} dt \, e^{\beta\sigma c t} \int_{4\pi} I \, d\hat{\Omega} + \frac{1 - e^{-\beta\sigma c\Delta t}}{c\sigma} S \, . \tag{14}$$

We note that Eq. (14) is equivalent to the time-dependent source and emission terms that the Carter-Forest method simulates via a Monte Carlo procedure.

Rather than solve the Carter-Forest equations, we make a consistent approximation to Eq. (14) by writing $\int dt I(t) \approx I(t)$ and incurring an $O(\Delta t)$ error:

$$u_{\mathrm{r}}^{n+1} = e^{-\beta\sigma c\Delta t} u_{\mathrm{r}}^{n} + \frac{1}{c} \left(1 - e^{-\beta\sigma c\Delta t} \right) \left(\int_{4\pi} I \, d\hat{\Omega} + \frac{1}{\sigma} S \right) \, , \tag{15}$$

or more compactly

$$u_{\mathrm{r}}^{n+1} = m_{\infty} u_{\mathrm{r}}^{n} + \frac{1}{c} \left(1 - m_{\infty} \right) \left(\int_{4\pi} I \, d\hat{\Omega} + \frac{1}{\sigma} S \right) \, , \tag{16}$$

with

$$m_{\infty} = e^{-\beta\sigma c\Delta t} \, . \tag{17}$$

As in the Fleck and Cummings method we have introduced an $O(\Delta t)\int_{4\pi} I\, d\hat{\Omega}$ error in going from Eq. (14) to Eq. (15).

Substituting the value of $u_{\rm r}^{n+1}$ given by Eq. (16) into the the transport equation we get

$$\frac{1}{c}\frac{\partial I}{\partial t} + \hat{\Omega}\cdot\nabla I + \sigma I = \frac{1}{4\pi}(1-m_\infty)\sigma\int_{4\pi} I\, d\hat{\Omega} + \frac{1}{4\pi}\left(c\sigma m_\infty u_{\rm r} + (1-m_\infty)S\right)\,. \tag{18}$$

Note the only difference in using the exact update for $u_{\rm r}^{n+1}$ is changing $f \rightarrow m_\infty$. We have the same definitions for the effective scattering and absorption, only evaluated with m_∞. The range and limits of m_∞ are the same as f; m_∞ is always in $[0,1]$ and limits to zero as $\Delta t \rightarrow \infty$.

3 Properties of m_∞

As noted above, the Fleck and Cummings method gives a first-order in time update of $u_{\rm r}^{n+1}$ when $\alpha = 1$. This can be shown by a Taylor expansion of f about $\Delta t = 0$

$$f = 1 - \beta\sigma c\Delta t + (\beta\sigma c\Delta t)^2 + O(\Delta t^3)\,. \tag{19}$$

The same Taylor series for m_∞ is

$$m_\infty = 1 - \beta\sigma c\Delta t + \frac{1}{2}(\beta\sigma c\Delta t)^2 + O(\Delta t^3)\,. \tag{20}$$

Comparing terms in these series we see that f approximates m_∞ to $O(\Delta t^2)$. This indicates that the Fleck and Cummings update for $u_{\rm r}^{n+1}$ is first-order in Δt. The method is first order because the convergence rate for a time-integration method is one order less than the order of the error for one time step due to the fact that error accumulates over several time steps [11].

The total error in a Fleck and Cummings time step is $\beta\sigma c O(\Delta t^2) + O(\Delta t)\int_{4\pi} I\, d\hat{\Omega}$ because of the approximation made in the time dependence of I. When f is replaced by m_∞ the error in one step is "just" $O(\Delta t)\int_{4\pi} I\, d\hat{\Omega}$.

As our numerical results will demonstrate, the factor m_∞ may cause the material temperature to change negligibly when large time steps are used. At large values of $\beta\sigma c\Delta t$ the linearization error in IMC is large. For large $\beta\sigma c\Delta t$ the change in $u_{\rm r}$ over a time step is negligibly small when m_∞ is used. The errors introduced by f allow $u_{\rm r}$ to change over a time step when $\beta\sigma c\Delta t$ is large. Of course it is possible that too much heating is allowed, producing nonphysical material temperatures. Our numerical results will show that m_∞ gives too little material heating and it is necessary to use a different factor than $m\infty$ for large time steps.

One way of constructing other orders of approximation to m_∞ is

$$m_l \equiv e^{-\beta\sigma c\Delta t} + \frac{1}{l}\frac{(\beta\sigma c\Delta t)^l}{(1+\beta\sigma c\Delta t)^{l+1}}\,. \tag{21}$$

Each m_l for l an integer, gives an $l^{\rm th}$ order approximation to m_∞. We demonstrate this point by noting that the Taylor series about $\Delta t = 0$ of the second term on the RHS of Eq. (21) gives

$$\frac{1}{l}\frac{(\beta\sigma c\Delta t)^l}{(1+\beta\sigma c\Delta t)^{l+1}} = O(\Delta t^l)\,, \tag{22}$$

that is, the rational expression in the definition of m_l adds an order l error.

Notice that the only difference between our IMC method and the Fleck and Cummings IMC method is in the difference between f and m_l. If these two factors were identical then our method would give the same result as standard IMC. The difference between f and m are presented in Figure 1. Also $f \leq m_l$, indicating that our modified IMC method always has more effective scattering than standard IMC. The difference in

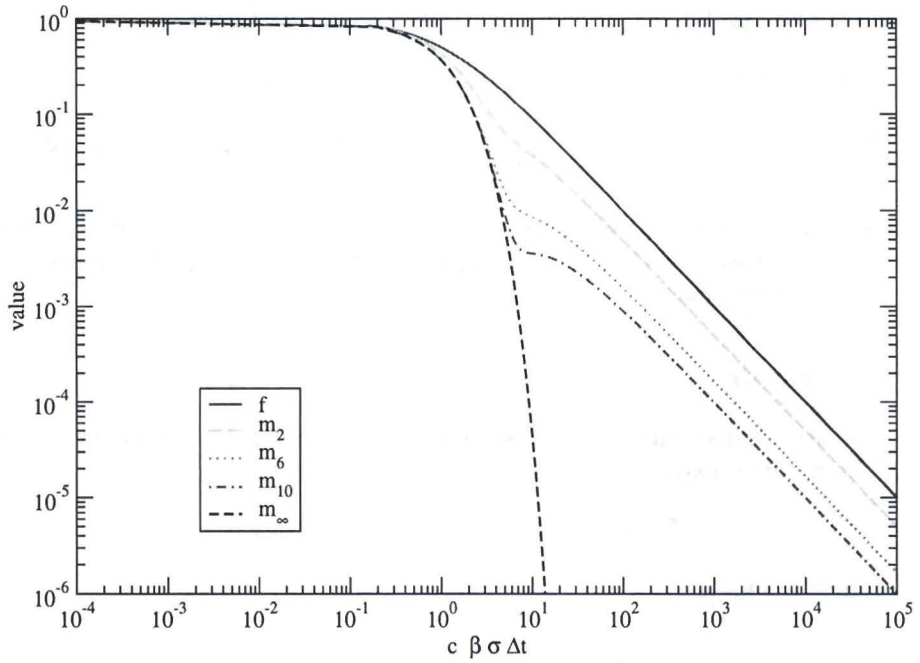

Figure 1: A comparison of the Fleck factor, f, and the m_l factors from the modified IMC method.

the amount of effective scattering is more pronounced when the time step is large compared to the time scale of the absorption/emission process.

Figure 1 also shows how the m_l values differ from m_∞ and f. The l value determines at which value of $\beta\sigma c\Delta t$ the m_l approximation breaks away from m_∞. For higher values of l, m_l matches m_∞ to larger values of $\beta\sigma c\Delta t$. After breaking away from the exponential curve of m_∞, m_l goes as $(\beta\sigma c\Delta t)^{-1}$, the same behavior as f.

As we shall see in our numerical results, in problems where the opacity is a function of the temperature, the smaller amount of heating in the m_l solutions can affect the evolution of the system, even when standard IMC does not cause overheating. In these cases it would be possible to use the standard f factor when $\beta\sigma c\Delta t$ is small and overheating is not an issue, and use m_l for an appropriate value of l when $\beta\sigma c\Delta t$ is large. On the other hand, using f or m_l with a small value of l can lead to nonphysical overheating of the material. We shall use these ideas to develop an adaptive method where l is chosen dynamically.

4 Equilibrium Diffusion Limit Analysis

The equilibrium diffusion limit of the thermal radiative transfer system, Eqs. (4), occurs when the opacity, σ, is large compared to the length scale on which I and u_m vary and the time-dependence of I and u_m and the source S are small compared to that same length scale (this in turn makes β large) [6,12]. The equilibrium diffusion limit can be arrived at by defining a small, positive parameter ϵ and scaling Eqs. (4) as

$$\frac{\epsilon}{c}\frac{\partial I}{\partial t} + \hat{\Omega}\cdot\nabla I + \frac{1}{\epsilon}\sigma I = \frac{1}{4\pi\epsilon}c\sigma u_\mathrm{r}\,, \tag{23a}$$

$$\frac{\partial u_\mathrm{r}}{\partial t} = \frac{1}{\epsilon^2}\beta\sigma\left(\int_{4\pi} I\,d\hat{\Omega} - cu_\mathrm{r}\right) + \beta S\,. \tag{23b}$$

and taking the limit as $\epsilon \to 0$ away from boundary and inital layers. This limit [12] gives the leading order intensity is a Planckian at the local temperature,

$$I^{(0)} = \frac{1}{4\pi} ac (T^{(0)})^4 \,, \tag{24}$$

where the superscript (0) denotes terms that are zeroth order in ϵ. The leading order temperature satisfies the nonlinear diffusion equation,

$$\frac{\partial}{\partial t} u_{\rm m}(T^{(0)}) + a \frac{\partial}{\partial t} (T^{(0)})^4 = \nabla \cdot \frac{ac}{3\sigma} \nabla (T^{(0)})^4 \,, \tag{25}$$

and the first moment in $\hat{\Omega}$ of the radiation intensity (generally called the radiation flux) is an order ϵ quantity given by

$$\left(\int_{4\pi} \hat{\Omega} I \, d\hat{\Omega} \right)^{(1)} = \frac{ac}{3\sigma} \nabla (T^{(0)})^4 \,. \tag{26}$$

To examine how our IMC method behaves in this limit we first look at m_l under the scaling $\sigma \to \sigma/\epsilon$ and $\beta \to \beta \to \beta/\epsilon$,

$$m_l \to \frac{\epsilon^2}{l \beta \sigma c \Delta t} + O(\epsilon^4) \,. \tag{27}$$

Thus, m_l is an $O(\epsilon^2)$ quantity. This implies that the effective scattering will be σ to leading order and that the effective absorption will be an order ϵ^2 quantity. In their analysis of the Fleck and Cummings IMC method, Densmore and Larsen [6] found the same scaling for the effective scattering and absorption. Therefore, their results for the equilibrium diffusion limit of the Fleck and Cummings method applies to our method as well.

Using the results of Densmore and Larsen, in the equilibrium diffusion limit our method solves the following diffusion equation

$$\frac{u_{\rm m}(T^{(0)}_{n+1}) - u_{\rm m}(T^{(0)}_{n})}{\Delta t} + \frac{1}{c} \frac{\phi^{(0)}_{n+1} - \phi^{(0)}_{n}}{\Delta t} = \frac{1}{\Delta t} \int_{t^n}^{t^{n+1}} dt \, \nabla \cdot \frac{1}{3\sigma} \nabla \phi^{(0)} \,, \tag{28}$$

where

$$\phi = \int_{4\pi} d\hat{\Omega} \, I \,, \tag{29}$$

and we have used subscripts to indicate time level. This equation is similar to Eq. (25) except that it does not enforce the equilibrium between ϕ and acT^4. This shortcoming of standard IMC in the equilibrium diffusion limit is not corrected by using a higher order approximation to $u_{\rm r}$. Nevertheless, we know that the two methods will behave similarly in this limit.

5 Frequency Dependent Case

The frequency dependent case poses no particular problems for developing a high order implicit Monte Carlo method. In this case the transport and material energy equations we wish to solve are

$$\frac{1}{c} \frac{\partial I_\nu}{\partial t} + \hat{\Omega} \cdot \nabla I_\nu + \sigma_\nu I_\nu = \frac{1}{4\pi} c \sigma_\nu b_\nu u_{\rm r} \,, \tag{30a}$$

$$\frac{\partial u_{\rm r}}{\partial t} = \beta \left(\int_0^\infty d\nu \int_{4\pi} d\hat{\Omega} \, \sigma_\nu I_\nu - c \sigma_{\rm p} u_{\rm r} \right) + \beta S \,, \tag{30b}$$

where $I_\nu(x, \hat{\Omega}, \nu, t)$ is the frequency-dependent specific intensity, and b_ν is the normalized Planck spectrum defined by

$$b_\nu = \frac{B_\nu}{u_{\rm r}} \,, \tag{31}$$

where the frequency-dependent Planck function is

$$B_\nu = \frac{2h\nu^3}{c^2}\left(e^{h\nu/kT}-1\right)^{-1}, \tag{32}$$

with h and k the Planck and Boltzmann constant's respectively. We have also defined the frequency-dependent opacity σ_ν and the Planck averaged absorption opacity as

$$\sigma_{\rm p} = \int_0^\infty b_\nu \sigma_\nu d\nu\,. \tag{33}$$

We integrate Eq. (30b) as in the grey case to write

$$u_{\rm r}^{n+1} = m_\infty u_{\rm r}^n + \frac{(1-m_\infty)}{c\sigma_{\rm p}}\left(\int_0^\infty d\nu \int_{4\pi} d\hat{\Omega}\,\sigma_\nu I_\nu + S\right) \tag{34}$$

where

$$m_\infty = e^{-\beta\sigma_{\rm p}c\Delta t}\,. \tag{35}$$

Upon substituting $u_{\rm r}^{n+1}$ from Eq. (34) into Eq. (30a) we get the linear transport equation

$$\frac{1}{c}\frac{\partial I_\nu}{\partial t} + \hat{\Omega}\cdot\nabla I_\nu + \sigma_\nu I_\nu = \frac{1}{4\pi}\frac{\sigma_\nu b_\nu}{\sigma_{\rm p}}(1-m_\infty)\int_0^\infty d\nu' \int_{4\pi} d\hat{\Omega}'\,\sigma'_\nu I'_\nu + \frac{cm\sigma_\nu b_v}{4\pi}u_{\rm r}^n + \frac{1}{4\pi}\frac{\sigma_\nu b_\nu}{\sigma_{\rm p}}(1-m_\infty)S\,. \tag{36}$$

In this equation the effective differential scattering cross-section is

$$\frac{d^2\sigma}{d\hat{\Omega}d\nu}(\nu'\rightarrow\nu) = \frac{1}{4\pi}\sigma'_\nu\frac{\sigma_\nu b_\nu}{\sigma_{\rm p}}(1-m_\infty)\,. \tag{37}$$

The total effective scattering and absorption cross-sections are given by integrating Eq. (36) over $\hat{\Omega}$ and ν to get

$$\sigma'_{\nu s} = (1-m_\infty)\sigma'_\nu\,, \tag{38}$$

$$\sigma'_{\nu a} = m_\infty\sigma'_\nu\,. \tag{39}$$

Similarly to Eq. (21) we can definite an approximation to m_∞

$$m_l = e^{-\beta\sigma_{\rm p}c\Delta t} + \frac{1}{l}\frac{(\beta\sigma_{\rm p}c\Delta t)^l}{(1+\beta\sigma_{\rm p}c\Delta t)^{l+1}}\,. \tag{40}$$

Equation (36) compares with the Fleck and Cummings IMC method for multifrequency problems where the transport equation solved is

$$\frac{1}{c}\frac{\partial I_\nu}{\partial t} + \hat{\Omega}\cdot\nabla I_\nu + \sigma_\nu I_\nu = \frac{1}{4\pi}\frac{\sigma_\nu b_\nu}{\sigma_{\rm p}}(1-f)\int_0^\infty d\nu' \int_{4\pi} d\hat{\Omega}'\,\sigma'_\nu I'_\nu + \frac{cf\sigma_\nu b_v}{4\pi}u_{\rm r}^n + \frac{1}{4\pi}\frac{\sigma_\nu b_\nu}{\sigma_{\rm p}}(1-f)S\,, \tag{41}$$

where

$$f = \frac{1}{1+\beta\sigma_{\rm p}c\Delta t}\,. \tag{42}$$

As in the grey case, the only difference between Fleck and Cummings IMC and our method is the factors f and m_l.

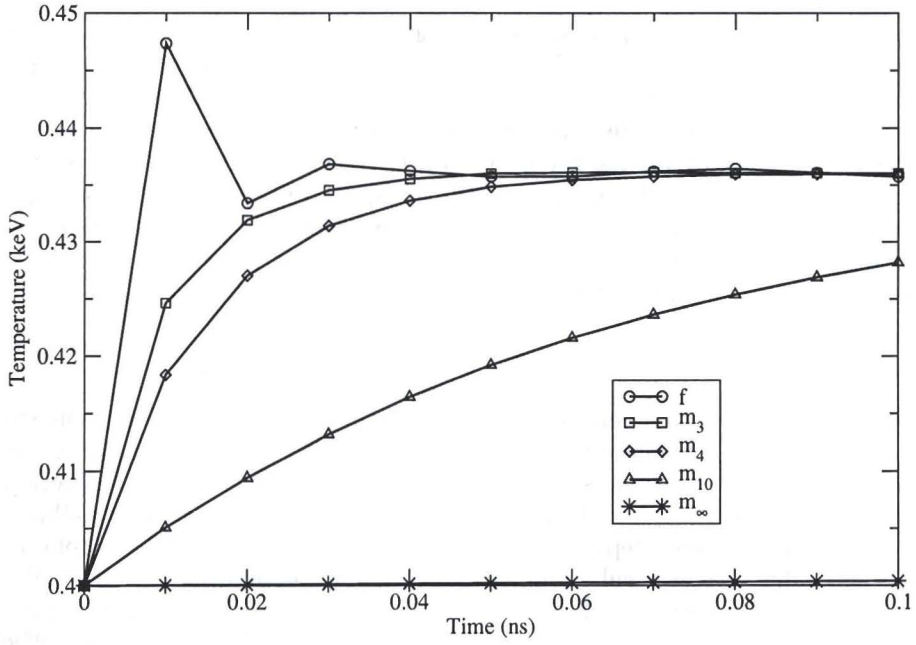

Figure 2: Infinite medium material temperature with initial $T_R = 0.5$ keV, $\Delta t = 0.01$ ns for different factors, either f or m_l.

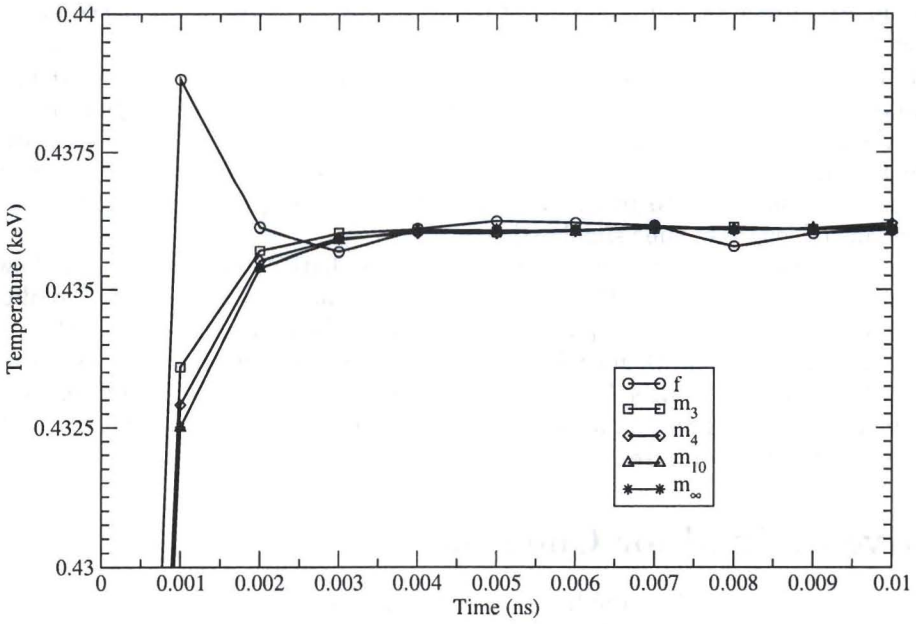

Figure 3: Infinite medium material temperature with initial $T_R = 0.5$ keV, $\Delta t = 0.001$ ns.

6 Comparison on 0-D Problems

We now compare methods using an infinite medium problem first explored by Densmore and Larsen [6]. In this problem there is a temperature-independent opacity of $\sigma = 100$ cm^{-1} and a temperature-independent heat capacity of $\rho c_v = 0.01$ GJ/cm^3-keV (1 GJ = 1 gigajoule = 10^9 J) and an initial material temperature of $T = 0.4$ keV. For units of time we use the nanosecond (10^{-9} s) and keV for temperature. Expressing physical constants in these units gives the speed of light, c, as 29.98 cm/ns, and the radiation constant, a as 0.01372GJ/cm^3-keV^4. For this problem, the mean-free time of a photon, $(c\sigma)^{-1}$, is 3.34×10^{-4} ns. The Fleck and Cummings results we obtain for this problem mirror those obtained by Densmore and Larsen.

In figures 2 and 3 the problem has the initial material temperature given by $T = 0.4$ keV and the initial radiation temperature as $T_R = 0.5$ keV, where

$$T_R = \sqrt[4]{\frac{\phi}{ac}}. \tag{43}$$

Figure 2 gives results obtained with a time step of $\Delta t = 0.01$ ns. In this figure, the time step size is much larger than the mean-free time, therefore we desire that the numerical results go to the equilibrium value of the material and radiation temperatures after one time step. At one extreme, the Fleck and Cummings solution, denoted in the figure by f, has the material temperature exceeding the equilibrium temperature after one time step. Successive time steps have the Fleck and Cummings solution nonphysically oscillating about the equilibrium value. These results for Fleck and Cummings indicate that it is allowing too much absorption in the first time step, causing the material to heat up too much. At the other extreme, the m_∞ solution only slightly heats up over the entire simulation time. For m_∞ there is too much effective scattering so there is no heating in the problem. The m_{10} solution is similar to the m_∞ solution in that there is not enough heating and the solution does not reach the equilibrium solution in the simulated time. The m_3 and m_4 solutions do not overshoot the equilibrium value and approach the equilibrium solution monotonically from below.

The consequences of decreasing the time step are shown in figure 3. Here the time step is $\Delta t = 0.001$ ns and $T_R = 0.5$ keV. This time step is still several mean-free times long. The Fleck and Cummings solution still overshoots the equilibrium temperature in the first time step and oscillates about the equilibrium thereafter. All of the m_l solutions for l finite approach the equilibrium solution from below and reach the equilibrium solution monotonically from below. The m_∞ solution remains near the initial material temperature.

Figure 4 shows results where the initial values of T_R and T are further out of equilibrium, $T_R = 0.7$ keV. In this problem the Fleck and Cummings solution overshoots the equilibrium value by about 17% and then oscillates about the equilibrium solution. The m_3 and m_4 solutions give a solution below the equilibrium value and take several time steps to reach the equilibrium. The m_{10} and m_∞ solutions never reach the equilibrium value in the length of time simulated.

Results for a large disparity in the initial material and radiation temperature are shown in figure 5. Here $T_R = 1.0$ keV. In this figure the Fleck and Cummings solution overshoots the equilibrium value by about 100% and does not get near the equilibrium value until the fourth time step. The m_3 solution also overheats in the first time step and then cools to the equilibrium solution. However, compared to the Fleck and Cummings solution it takes longer for the m_3 solution to reach the equilibrium temperature. The m_4 solution is within 1% of the equilibrium solution in the first time step. Finally, the m_{10} and m_∞ solutions underpredict the material temperature.

7 Adaptive Method for Choosing l

The 0-D results presented above show the benefits to the modified method, and the drawbacks to standard IMC. The question of how to pick l is still open; in the 0-D cases, no single selection of l was ideal for every problem. However, we can *a priori* decide which l will work best for a given infinite medium problem.

To choose the appropriate value of l we first determine if $T_R > T$. If so, then the material temperature could overshoot the equilibrium temperature. If $T > T_R$, then material overheating cannot occur and we

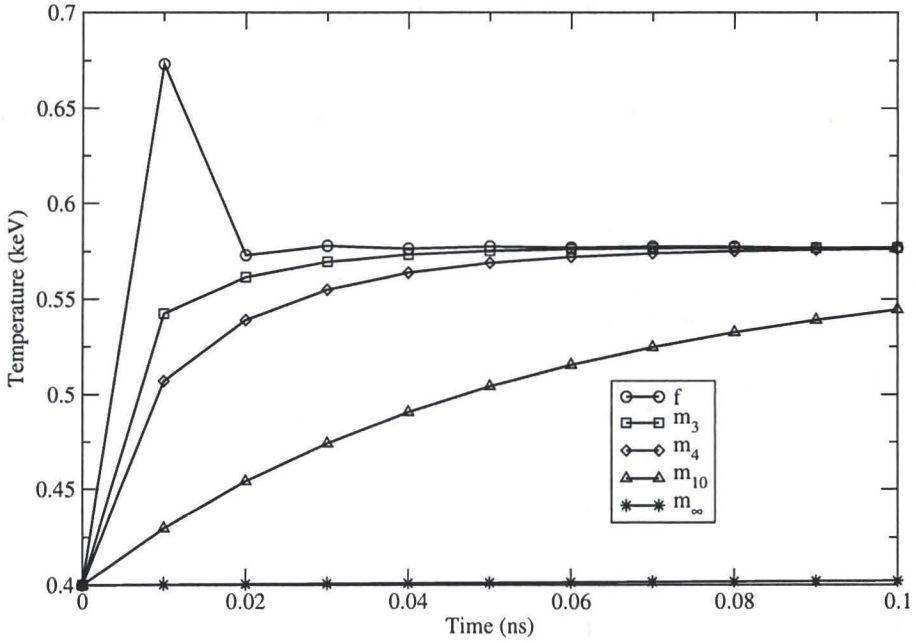

Figure 4: Infinite medium material temperature with initial $T_{\mathrm{R}} = 0.7$ keV, $\Delta t = 0.01$ ns.

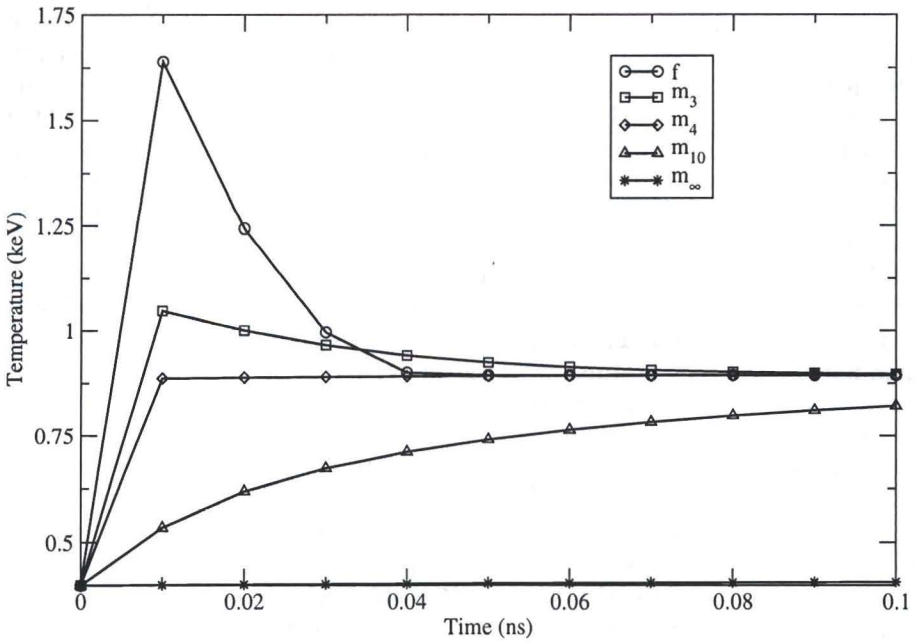

Figure 5: Infinite medium material temperature with initial $T_{\mathrm{R}} = 1.0$ keV, $\Delta t = 0.01$ ns.

can use standard IMC. When $T_{\mathrm{R}} > T$, we then determine if this overshoot occurs by solving a 0-D problem. For a 0-D problem, IMC has the solution for the material energy given by [5]

$$u_{\mathrm{m}}^{n+1} = u_{\mathrm{m}}^{n} + \left(a(T_{\mathrm{R}}^{n})^4 - u_{\mathrm{r}}^{n}\right)\left[1 - e^{-f\sigma c\Delta t}\right]. \tag{44}$$

We can determine T_{n+1} from u_{m} via the equation of state and compare it to the equilibrium temperature, T_{eq}, which is found by solving

$$a(T_{\mathrm{R}}^{n})^4 + u_{\mathrm{m}}^{n} = aT_{\mathrm{eq}}^4 + u_{\mathrm{m}}(T_{\mathrm{eq}}). \tag{45}$$

If T_{n+1} is greater than T_{eq}, then we recompute T_{n+1} using m_2 instead of f. If m_2 overshoots the equilibrium temperature, then we increase l until $T_{n+1} \leq T_{\mathrm{eq}}$.

We use a similar procedure for multidimensional problems. In this case we solve a 0-D problem in each computational cell. The 0-D problem we solve has the radiation temperature given as the maximum of the radiation temperature in the cell and the temperatures (both radiation and material) in its neighboring cells. This takes into account the fact that energy can move between cells. Using data from neighboring cells should be effective when the cells are optically thick. It is precisely in the case of optically thick cells that overheating can be a problem; thin cells will most likely not have too much absorption in a time step. Also, for multidimensional problems we set a user specified maximum value for l. We allow such a maximum because the 0-D solution can be too restrictive in suppressing material heating and force l to be larger than needed for multidimensional problems.

8 Multidimensional Results

Our adaptive scheme for choosing the integration order was implemented in the `Milagro` implicit Monte Carlo code developed at Los Alamos National Laboratory [13]. To demonstrate the effectiveness of the adaptive scheme we solve a problem relevant to inertial confinement fusion using an indirect drive, hohlraum configuration. The layout of the problem is due to Brunner [14], though we have changed the problem from planar geometry to cylindrical $r - z$ geometry. The layout of the problem is shown in Fig. 6.

In Fig. 7 we compare the solutions from standard IMC with our adaptive scheme with a maximum integration order of 3 with fixed time step sizes. All problems used 5×10^5 particles per time step initially, ramping up to 10^6 particles per time step by the end of the simulation; the computational mesh has uniform spacing of 65 cells in the r direction and 260 cells in the z direction. In Fig. 7 there is noticeably less noise in the adaptive solution than in standard IMC. The reduced noise is a result of there being more effective scattering in those regions of the problem where the integration order is increased. Also, we notice that in the $\Delta t = 0.01$ ns solution the temperature wave has propagated slightly farther into the central block in the standard IMC solution.

The effect of the adaptive scheme on the maximum material temperature as a function of time is shown in Fig. 8. This figure demonstrates that standard IMC has the maximum temperature above the 1 keV drive temperature for most of the problem. The adaptive scheme does not completely eliminate this overheating, but the maximum nonphysical temperatures with the adaptive scheme are smaller than standard IMC.

The differences in the initial heating transient are demonstrated by the plots of the temperature as a function of time at the fiducial points in Figs. 9 and 10. At $(r, z) = (0.005, 0.105)$, a point that is directly irradiated by the boundary source, the standard IMC solution overshoots the drive temperature in its early transient. The adaptive scheme solution has a monotonic transient, with both sizes of time step. At the point $(r, z) = (0.44, 0.56)$ the transient from 0 to 1 ns has the same behavior for the different methods but different rise times. The adaptive scheme's results heat up more slowly than standard IMC for a given time step. We do note that in terms of the entire solution time, this slight change in transient behavior is a minor effect. Outside the transient region all methods converge to the same temperature.

Turning to geometric comparisons of the solutions, Figs. 11 and 12 show the material and radiation temperatures at $t = 10$ ns and $r = 0.005$ cm. The material temperatures in Fig. 11 are in general agreement between the two methods. The largest discrepancy is near $r = 0.6$ cm where the standard IMC solution with $\Delta t = 0.01$ ns. This could be attributed to solution noise. The radiation temperature solutions are also mostly

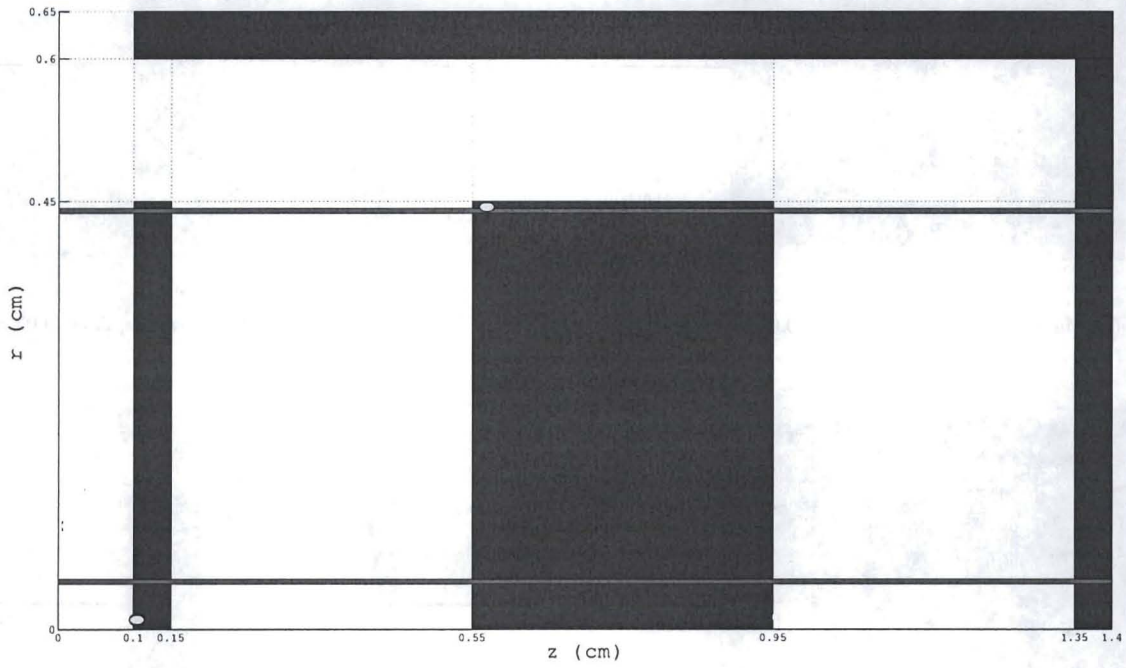

Figure 6: Layout for the hohlraum problem: the shaded regions have $\sigma = 300T^{-3}\,\mathrm{cm}^{-1}$ with T in keV, $\rho c_v = 0.3$ GJ/cm^3-keV; the white regions are vacuum. There is a 1 keV boundary source at $z = 0$, and the problem is initially cold. The lines at $r = 0.05$, 0.44 and the dots at $(r, z) = (0.005, .105)$ and $(0.44, 0.56)$ indicate areas were we look at the solution in detail in later figures.

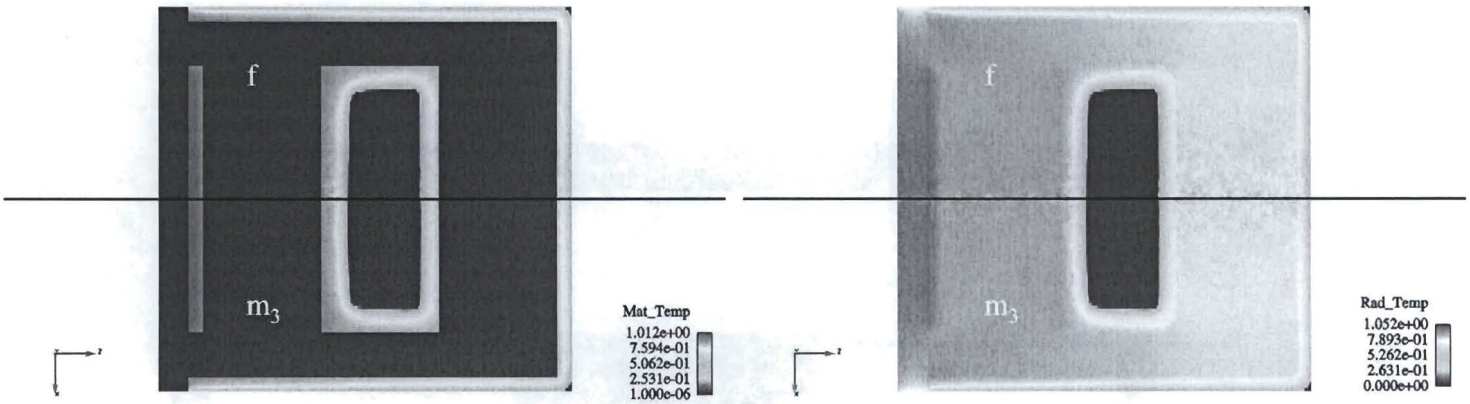

(a) Material Temperature, $\Delta t = 0.05$ ns

(b) Radiation Temperature, $\Delta t = 0.05$ ns

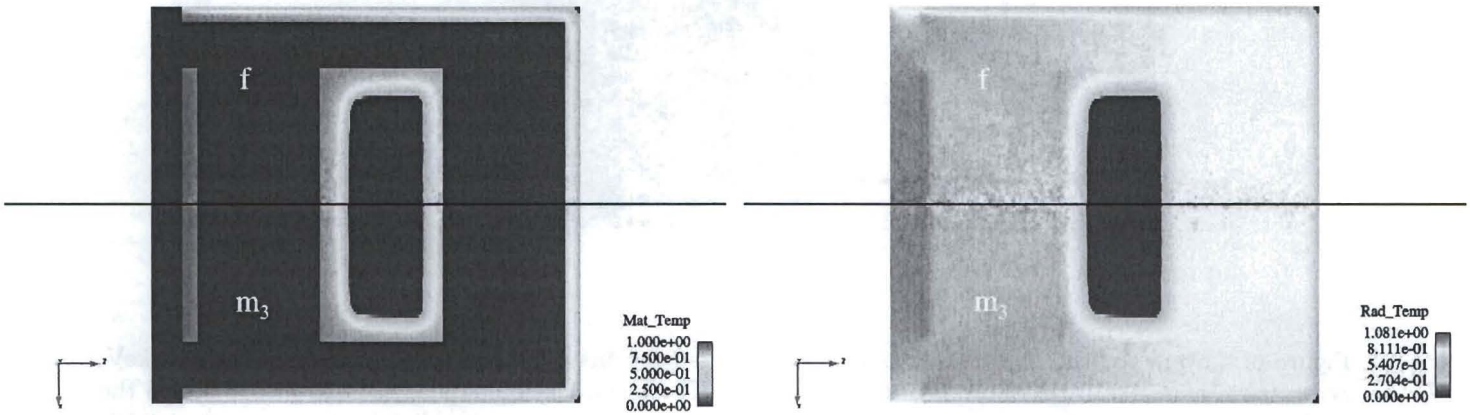

(c) Material Temperature, $\Delta t = 0.01$ ns

(d) Radiation Temperature, $\Delta t = 0.01$ ns

Figure 7: Results for the hohlraum problem at $t = 10$ ns. The top and bottom halves of each subfigure are, respectively, the standard IMC solution and the adaptive solution with the maximum l set to 3.

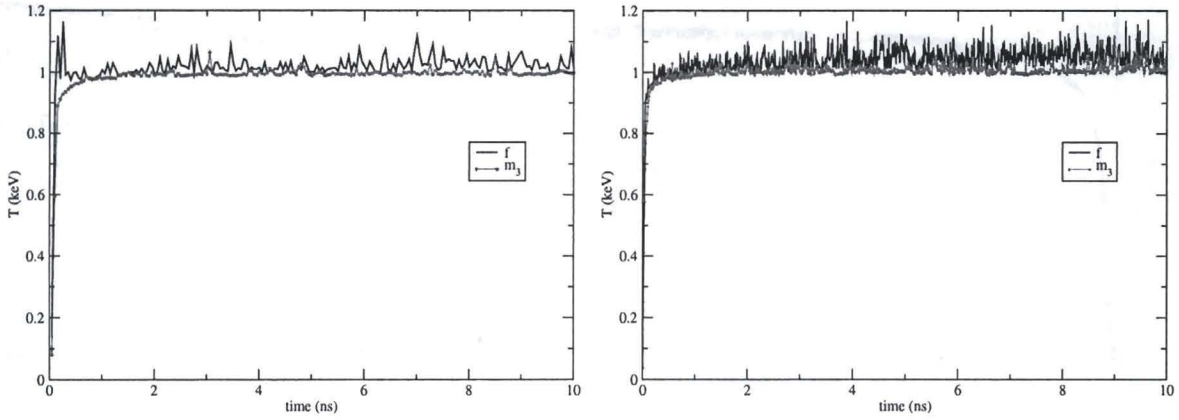

(a) $\Delta t = 0.05$ ns (b) $\Delta t = 0.01$ ns

Figure 8: Comparison of the maximum material temperature for the adaptive scheme and standard IMC.

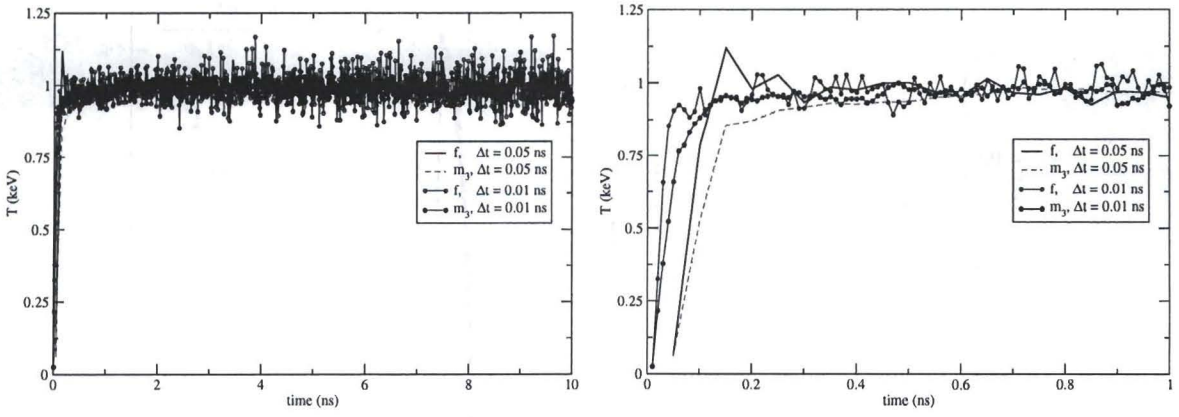

(a) (b) Detail from 0 to 1 ns

Figure 9: The material temperature as a function of time at $(r, z) = (0.005, 0.105)$.

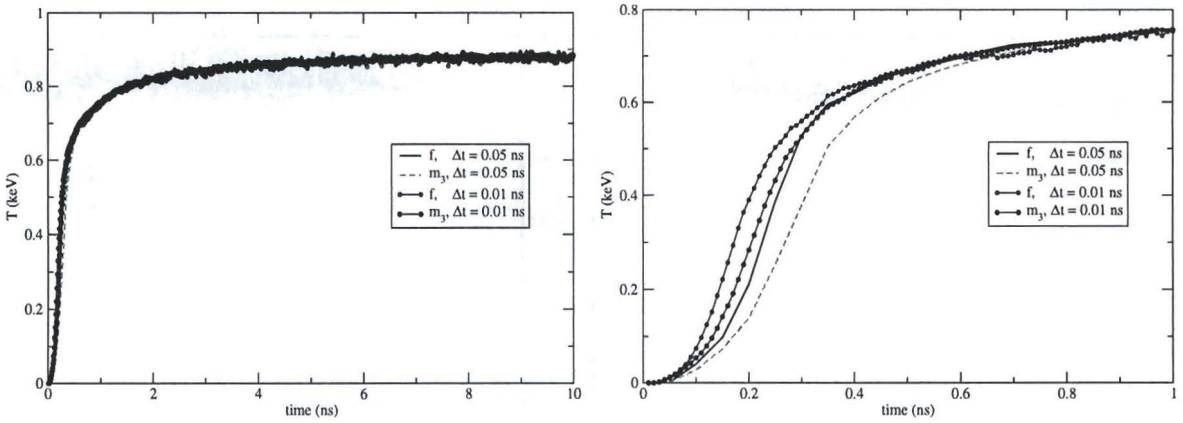

(a) (b) Detail from 0 to 1 ns

Figure 10: The material temperature as a function of time at $(r, z) = (0.44, 0.56)$.

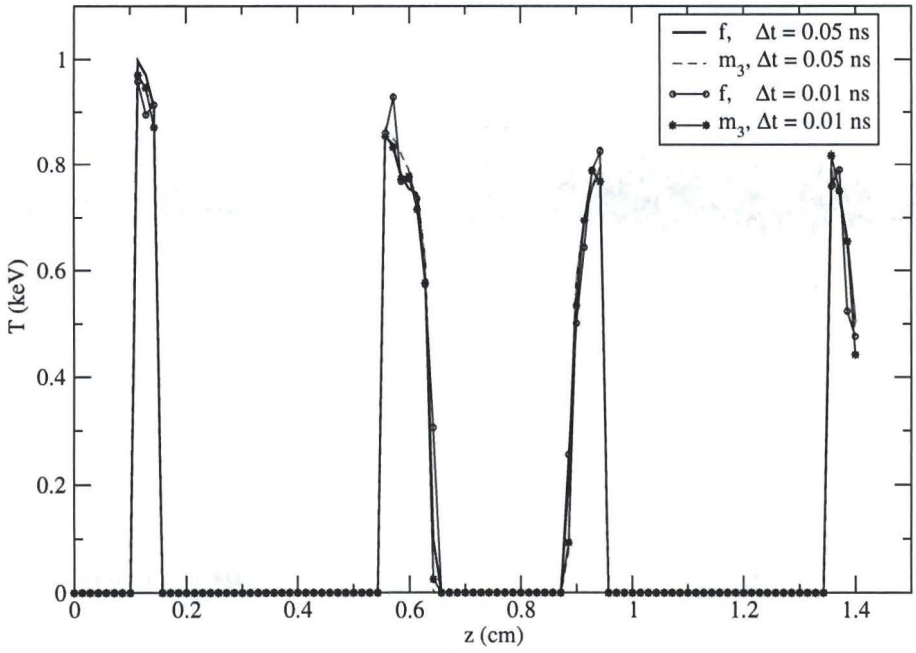

Figure 11: The material temperature at $r = 0.05$ cm, $t = 10$ ns.

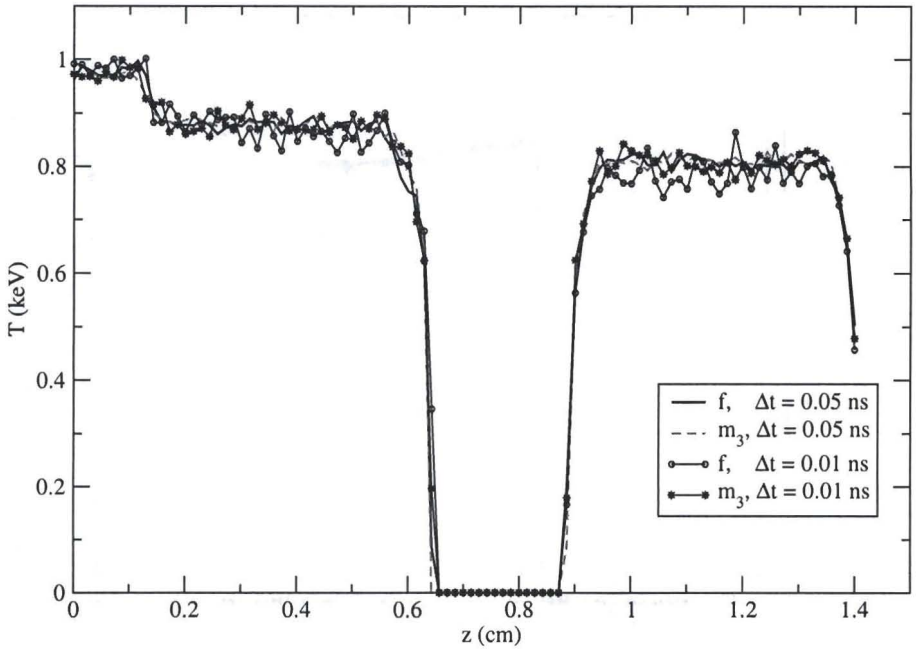

Figure 12: The radiation temperature at $r = 0.05$ cm, $t = 10$ ns.

in agreement, though the small time step solution with standard IMC is plagued by noise. Finally, along the line at $r = 0.44$ cm the material temperatures are in general agreement across all solutions (c.f. Fig.13).

9 Conclusions

We have presented a new implicit Monte Carlo method, in both gray and multifrequency treatments, that provides a framework to suppress the nonphysical overheating that can occur in the standard Fleck and Cummings IMC method when large time steps are used. The method we have presented has the same properties in the diffusion limit as standard IMC. In its implementation this new method differs from Fleck and Cummings IMC method only in the changing of the f factor to an m_l factor.

Infinite medium numerical results demonstrated how the choice of the integration order, l, effects the amount of heating as a function of time. Where standard IMC nonphysically overheated the material and then had the material temperature oscillate around the equilibrium temperature, the modified IMC solutions with the Fleck factor replaced by m_l approached the equilibrium temperature monotonically. For large initial differences in the radiation and material temperatures, the m_l solution did overshoot the equilibrium temperature for $l = 3$.

Inspired by the infinite medium results, we developed an adaptive scheme to suppress the overheating that can be present in standard IMC. The adaptivity is based on solving a 0-D problem in each computational cell; where the solution to the 0-D problem indicates that overheating could occur, we adjust the integration order to prevent the overheating.

On a multidimensional problem, we showed that using the adaptive method suppressed most of the overheating that was found in the standard IMC solution. Moreover, the adaptive solutions had less noise than standard IMC for the same number of particles, an effect due to the added scattering in the problem. Though the behavior in transients was changed and the amount of noise differed, both the adaptive scheme and standard IMC gave solutions that were mostly in agreement at late times.

In the future we will investigate combining our method with semi-implicit ideas of Gentile [7] that include the variation of the opacity with temperature in the linearization. Including the opacity in the linearization

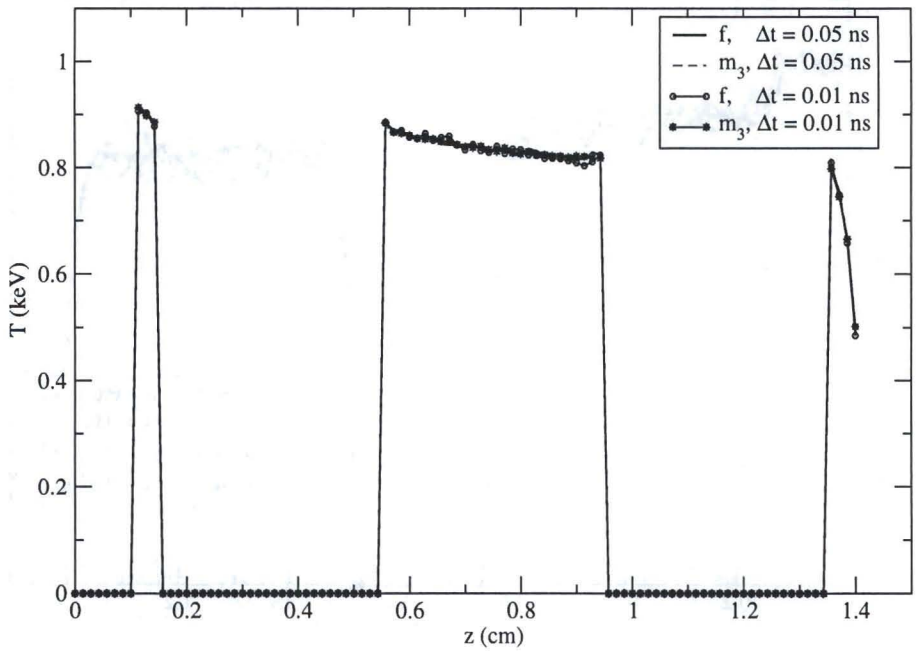

Figure 13: The material temperature at $r = 0.44$ cm, $t = 10$ ns.

is compatible with our method and should enhance the method's robustness. We also plan on exploring the idea of solving a 0-D problem in each cell to prescribe a time step control rather than changing the integration order. Beyond these extensions we hope to apply our method to radiation-hydrodynamics simulations of astrophysical phenomena and interial confinement fusion.

References

[1] J. A. Fleck, Jr. and J. D. Cummings, "An implicit Monte Carlo scheme for calculating time and frequency dependent nonlinear radiation transport," *J. Comp. Phys.*, vol. 8, pp. 313–342, 1971.

[2] E. W. Larsen and B. Mercier, "Analysis of Monte Carlo method for nonlinear radiative transfer," *J. Comp. Phys.*, vol. 71, pp. 50 – 64, 1987.

[3] E. S. Andreev, M. Y. Kozmanov, and E. B. Rachilov, "Maximum principle for a system of equations of energy and non-stationary radiation transfer," *U.S.S.R. Comput. Math. Math. Phys.*, vol. 23, no. 104, 1983.

[4] B. Mercier, "Application of accretive operators theory to the radiative transfer equations," *SIAM J. Math. Anal.*, vol. 18, no. 2, pp. 393–408, 1987.

[5] S. W. Mosher and J. D. Densmore, "Stability and monotonicity conditions for linear, grey, 0-D implicit Monte Carlo calculations," *Trans. Am. Nuc. Soc.*, vol. 93, p. 520.

[6] J. D. Densmore and E. W. Larsen, "Asymptotic equilibrium diffusion analysis of time-dependent Monte Carlo methods for gray radiative transfer," *J. Comp. Phys.*, vol. 199, pp. 175–204, 2004.

[7] N. A. Gentile, "A comparison of various temporal discretization schemes for infinite media radiation transport," *Trans. Am. Nuc. Soc.*, vol. 97, p. 544, 2007.

[8] L. L. CARTER and C. A. FOREST, "Nonlinear radiation transport simulation with an implicit Monte Carlo method," Tech. Rep. LA-5038, Los Alamos National Laboratory, 1973.

[9] E. D. BROOKS, III, "Symbolic implicit Monte Carlo," *J. Comp. Phys.*, vol. 83, p. 433, 1989.

[10] T. N'KAOUA, "Solution of the nonlinear radiative transfer equations by a fully implicit matrix Monte Carlo method couple with the Rosseland diffusion equation via domain decomposition," *SIAM J. Sci. Stat. Comput.*, vol. 12, p. 505, 1991.

[11] K. DEKKER and J. G. VERWER, *Stability of Runger-Kutta methods for stiff nonlinear differential equations.* Amsterdam: Elsevier-North Holland, 1984.

[12] E. W. LARSEN, G. C. POMRANING, and V. C. BADHAM, "Asymptotic analysis of radiative transfer problems," *J. Quant. Spec. and Rad. Transfer*, vol. 29, no. 4, 1983.

[13] T. J. URBATSCH and T. M. EVANS, "Milagro version 2, an implicit monte carlo code for thermal radiative transfer: capabilities, development, and usage," Tech. Rep. LA-14195-MS, Los Alamos National Laboratory, January 2005.

[14] T. A. BRUNNER, "Forms of approximate radiation transport," Tech. Rep. SAND2002-1778, Sandia National Laboratories, July 2002.

RGM:rgm
Distribution:
Jayenne Project Team,
Robert Lowrie/CCS-2 D413
Ed Dendy/CCS-2 D413